

Electronic Supplementary Information (ESI):

## **Solvent-mediated Isotope Effects Strongly Influence the Early Stages of Calcium Carbonate Formation: Exploring D<sub>2</sub>O vs. H<sub>2</sub>O in a Combined Computational and Experimental Approach**

Michael King, Jonathan T. Avaro, Christine Peter, Karin Hauser and Denis Gebauer

### **Contents**

<b>Experimental</b> .....	<b>1</b>
<i>Computational Methods</i> .....	1
Cluster Size and Lifetime .....	2
Residence Time .....	3
Parameterization.....	3
<i>Titration Experiments</i> .....	4
Devices, general titration and calibration procedure.....	4
Determination of equivalent pH in the different aqueous solvents .....	5
<i>Fourier-Transform Infrared Spectroscopy (FTIR)</i> .....	6
Rapid Scan Measurements .....	6
<b>Supplementary Tables</b> .....	<b>7</b>
<b>Supplementary Figures</b> .....	<b>9</b>
<b>References</b> .....	<b>14</b>

### **Experimental**

#### ***Computational Methods***

The algorithms described below were created and implemented as in-house python scripts if not mentioned otherwise. In the following, we describe the analyses of the ion clusters by following them over the course of the trajectory and calculating their size and lifetime. The simulations using *H<sub>2</sub>O* as solvent – pure solvent or a *CaCO<sub>3</sub>* solution – were performed in LAMMPS with the force field of Raiteri et al.<sup>1</sup> The simulations using *D<sub>2</sub>O* as solvent used the same general force field settings as in the *H<sub>2</sub>O* case. The change in the interaction parameters for the *D<sub>2</sub>O* model is described below. NPT simulations were run with a 1 fs time step, a Nosé-Hoover chain thermostat with a chain length of 5 and a 100 fs relaxation

time, and a barostat of chain length 5 and a 1000 fs relaxation time.<sup>2,3</sup> Electrostatic interactions were computed with the PPPM algorithm<sup>4</sup> with an accuracy of  $10^{-5}$ .

### Cluster Size and Lifetime

*Identifying the clusters and calculating their size.* The cluster ids are calculated by distance based clustering. In a distance based clustering, a unique number (cluster id) is assigned to a group of atoms whose inter-atomic distances are below a certain cutoff. At the beginning of each frame, the cluster id is set to the atom id. One iterates over all atoms and compares the cluster id with the one of all other atoms. If the cluster ids differ, the distance between both atoms is calculated. If the distance is below the cutoff, the cluster id of both atoms will be set to the lower one of both. It will be registered that a change occurred. If at the end of the iteration, any change between the cluster ids was registered the procedure will be repeated until no changes occur. This algorithm can be improved by including all atoms from one molecule in one cluster or introducing other constraints. In the basic form it is available within LAMMPS. The algorithm was also implemented in python and, therefore, is easily extendable. The cluster size can be directly calculated by creating a histogram of the cluster ids at each time frame.

*Removing small fluctuations of the cluster members.* Artifacts of a plain cutoff were reduced by a smoothing of the property "cluster id/atom/frame" over multiple frames: A window of 10 frames was moved over the data. Over the window, it is counted how often an atom is member of a specific cluster. If the atom is a member of a specific cluster during 70 % of the time, it is assigned to this cluster id (otherwise 0). In the smoothed data, small fluctuation of the clusters are removed.

*Following the clusters over the course of a trajectory.* A unique cluster id over the whole trajectory is required to follow the development of a cluster over the course of a trajectory. The previously described clustering algorithm leads to a unique id per frame but not per trajectory. In the following, only clusters with at least 2 members are recorded. The unique cluster ids at the last time step are stored in a dictionary. The trajectory is then processed in reverse order. For every frame, the unique cluster ids of clusters above the minimum size are extracted. A new empty dictionary is created. For every cluster, the set of members is compared with the previously stored sets of the different clusters. The intersection between the sets is calculated and the stored cluster id of the set with the biggest intersection is further used. If the intersection is above half of the set size, the search is directly aborted. If no matching cluster is found, a new unique cluster id is assigned to the cluster and it is stored in the dictionary. Otherwise, if a matching cluster is found in the previous frame, it is checked if its already present in the new dictionary. If it is not, it is assigned the cluster id of the previous frame. If the cluster id is already present in the dictionary of the current step, a new cluster id is assigned. This allows the handling of merging and splitting events. The cluster ids are stored in an array with an id per atom and frame.

*Calculation of the lifetime of a cluster.* The lifetime of a cluster can be calculated for an individual cluster by following it over the course of the trajectory. An array with a unique cluster id per occurrence of the cluster in the whole trajectory is needed, as described above. For every frame the number of members in the cluster is evaluated. If it is above a

given value, e.g., two for ion pairs, it is counted. The lifetimes of the individual clusters are then binned in a histogram.

### Residence Time

*Calculation of the residence time via bookkeeping of the coordination shell.* The residence time of water around ions is calculated via bookkeeping of the water molecules around a single ion in solution. To this end, two cutoff radii are defined, an inner cutoff radius for the first solvation shell and an outer cutoff radius for the second shell. The values are 3.0 Å & 5.4 Å for  $Ca^{2+}$  and 4.25 Å & 6.4 Å for  $CO_3^{2-}$ . The residence time of every water molecule within the first shell is accumulated until the water molecule leaves the outer cutoff (second solvation shell). This allowed a short-term movement of water molecules between the first and second shell. The mean and standard deviation of all the accumulated times is then calculated.

*Calculation of the residence time via time correlation function.* Another method to calculate the residence time was introduced by Impey et al.<sup>5</sup> with a good description found in Koneshan et al.<sup>6</sup> The residence time was calculated from the time correlation function via integration:

$$R(t_n, t) = \frac{1}{N_h} \sum_{i=1}^{N_h} P_i(t_n, t; t^*)$$

$$\tau_{Impey} = \int_0^{\infty} \langle R(t) \rangle dt$$

$N_h$  is the number of water molecules in the coordination shell at time point  $t_n$ .  $P_i(t_n, t; t^*)$  is a function that returns 1 if the  $i$ th molecule is within the coordination shell at time point  $t_n$  and  $t_n + t$  and returns 0 otherwise. The excursion of a water molecule from the first solvation shell for several time steps is allowed by the parameter  $t^*$  and set to  $\leq 2$  ps as used by Impey et al.<sup>5</sup> The trajectory is split into multiple parts to obtain different starting points  $t_n$ . The residence time is then obtained by the integration over time of the expectation value of  $\tau_{Impey}$ . The expectation value is obtained by averaging over different starting points  $t_n$ . Koneshan et al. suggested a numerical integration for the first 10 ps along with an exponential fitting of  $\exp(-t/\tau)$  and analytical integration on the remaining data.<sup>6</sup> In our case, the difference between a pure numerical solution and fitted solution is around 3%, we thus report the data obtained from the fitting results. The coordination shell was defined for water molecules within 3.39 Å for  $Ca^{2+}$ , as used by Koneshan et al., and 4.25 Å for  $CO_3^{2-}$ . The trajectory was split into 40 windows to obtain different time points  $t_n$ .

### Parameterization

A flexible heavy water model was created in analogy to the work of Grigera.<sup>7</sup> Grigera developed a heavy water model by reparameterizing the electrostatic interactions in the SPC/E water model.<sup>8</sup> We calculated the ratio how the charges of the SPC/E model were scaled to obtain the SPC/HW model. The same scaling was done for the SPC/fw model.<sup>9</sup> The new flexible heavy water model is named SPC/HW/fw. The parameters of the different water models are shown in Table S1.

*Radial distribution function of water.* The radial distribution functions of the different atom types in  $H_2O/D_2O$  were calculated and are shown in Figure S1. The sharpness of the first peak of O–O is in good agreement with the values obtained for the rigid  $D_2O$  model (SPC/HW). Also, the H–H and O–H values are in a good agreement (Figure S1). The shifts of peaks from SPC/fw to SPC/HW/fw are in the same range as the shifts from SPC/E to SPC/HW.

*Properties of the heavy water model.* Furthermore, different water properties were calculated for the validation of the approach (Table S2). The mean value of the H-O-H angle of 107.2 fits well to the angle of 106 found in experiments and also used in the SPC/HW model (107.7). However, the bond lengths of both the  $H_2O$  and  $D_2O$  model are slightly too large and the shortening for  $D_2O$  is not covered. On the other hand, the tetrahedrality  $\langle q \rangle$  increases from  $D_2O$  to  $H_2O$  as expected. The densities of the  $D_2O$  model is  $1.139 \text{ gcm}^{-3}$ , compared to 1.104 obtained by experiments and 1.125 from the SPC/HW model. The electric dipole moments  $\mu$  of the  $D_2O$  and  $H_2O$  model were calculated and the ratio of the dipole moments,  $\mu_{D_2O}/\mu_{H_2O}$ , can be set in relation to the ratio of the experimentally obtained polarizabilities of  $H_2O/D_2O$ . The ratio of 1.03 is in good agreement with experimental value of the 1.05 and the ratio for SPC/E vs SPC/HW of 1.03.

*Solvent structure around  $Ca^{2+}$  and  $CO_3^{2-}$  ions.* The radial distribution function and coordination numbers of ions in  $D_2O$  are in a good agreement with the ones of water (Figure S2). A slight shift of the maxima can be measured, for  $Ca^{2+}$  from 2.355 to 2.345 Å and for  $CO_3^{2-}$  from 3.225 to 3.235 Å.

*Summary and outlook on the  $D_2O$  model.* For the present work, only water–water interactions were changed in the switch from  $H_2O$  to  $D_2O$ . In an extension of this work the water–ion interactions could be revisited – an endeavor that goes well beyond the present work. The results could further be checked by creating a  $D_2O$  model without changing the charges. Yet, the simulations of several alternative models and the work of Glättli<sup>10</sup> showed that the most promising way to create a  $D_2O$  model is indeed the scaling of the charges. In contrast, changing other properties such as intramolecular interactions or van der Waals interactions leads to a change of some properties towards  $D_2O$  and of others in the opposite direction. Thus, for the present work we decided to use a  $D_2O$  model with scaled charges.

## **Titration Experiments**

### Devices, general titration and calibration procedure

In order to avoid unwanted  $H_2O$  diffusing into the  $H_2O/D_2O$  mixtures, the complete potentiometry experimental apparatus was put in a glove box purchased from SICCO (SICCO Glove box, PMMA – V1984-08), The glove box was first filled with nitrogen at a flow rate of 30 litres per minute and then constantly purged with nitrogen at a rate of 2 litres per minute in order to maintain an oxygen-free atmosphere. In all experiments  $D_2O$  (99%) from Sigma Aldrich was used. All  $D_2O$  containing solutions were prepared based on more concentrated stock solutions prepared outside the glove box in pure  $H_2O$  so as to achieve the desired concentration depending on the targeted  $D_2O$  content. Once prepared, the solutions were transferred to the glove box where  $D_2O$  was finally added to set the reactant

concentration to 10mM. Samples containing 99% D<sub>2</sub>O were all prepared under nitrogen atmosphere in the glove box.

For each measurement, the titration vessel was filled with 10 mL of 10 mM carbonate buffer at different D<sub>2</sub>O content (0%, 12.5%, 25%, 50%, 75%, 99% v/v). A fresh calcium stock solution containing similar H<sub>2</sub>O/D<sub>2</sub>O was then slowly dosed (0.01mL/min) into a sodium carbonate solution of variant D<sub>2</sub>O ratios using a Titrando 951 titration device operating two Dosino 800 dosing units. The titration setup was controlled by the software Tiamo version 2.5, which allows simultaneous and precise dosing of reactant solutions, controlling pH and reading out the voltage of the electrodes.

The pH was finely adjusted to pH 9.00 in water (*cf.* next section) by adding small increments of 100 mM sodium hydroxide solution (Alfa Aesar 35620) to the sodium bicarbonate solution. After each experiment, the titration vessel and electrodes tips were thoroughly washed with acetic acid (10%), Milli-Q water and dried with dust-free tissue paper. Milli-Q and acetic acid flasks were kept in the glove box and sealed with parafilm to avoid any H<sub>2</sub>O-water vapor atmosphere contamination.

The calcium potential and pH at different H<sub>2</sub>O/D<sub>2</sub>O ratios were recorded using a polymer-membrane-based calcium ion selective electrode (ISE, Metrohm 6.0508.110) and glass electrodes (Metrohm Unitrode flat membrane 6.0256.100) with internal reference, respectively. The internal reference system of the pH electrode was also used as reference for the calcium ISE. Added volumes and potentials were automatically recorded every 10 seconds during the titration experiments. The calcium ion selective electrode was calibrated by titration of 10 mM calcium chloride solution into ultrapure water containing targeted H<sub>2</sub>O-D<sub>2</sub>O ratios. A three-point calibration of the pH electrodes was performed using standard pH buffer solutions from Mettler-Toledo with the product numbers: pH = 4.01: 51302069; pH = 7.00: 51302047; pH = 9.21: 51302070.

#### Determination of equivalent pH in the different aqueous solvents

Due to the change of the acid constants of the carbonate buffer as well as the change of the self-dissociation constant between D<sub>2</sub>O and H<sub>2</sub>O (*cf.* the introduction of the article), the pH and pD values cannot be directly compared, at least when it comes to calcium carbonate formation. Thus, here, we give the pH (that is, of the pure light water solution), and adjusted the formal pH of the different solvent mixtures to an equivalent value, at which the ratio of carbonate and bicarbonate ions is the same as in pure light water. This is what we call the equivalent pH. To this end, the pK<sub>2</sub> value of carbonate ions in the different D<sub>2</sub>O/H<sub>2</sub>O mixtures was experimentally established via slow addition of sodium hydroxide (NaOH = 0.1M) to a sodium carbonate solution (Na<sub>2</sub>CO<sub>3</sub> = 0.01M), initially set to pH 12 and containing 12.5%, 25%, 37.5%, 50%, 75% and 99% D<sub>2</sub>O. The pK<sub>a</sub> value of the carbonate ion in the different environments was identified for each of the different D<sub>2</sub>O contents at the inflection point of the pH curve present between pH 10.33 and 10.8. These experimental pH values can then be converted using the formula given by Salomaa et al.<sup>11</sup>:

$$pL = pH + 0.3314n + 0.0766n^2;$$

where pL is the generalized equivalent of pH in the mixture (including all the isotopically different hydrogens), pH the pH meter reading and n the fraction of deuterium in the

mixture. The as-obtained pKa values (Table S3) of the carbonate ion can be contrasted with those obtained via the formula of Krężel and Bal<sup>12</sup>:

$$\text{pKa} = 0.929 \text{ pK}^{\text{H}^*} + 0.42;$$

where  $\text{pK}^{\text{H}^*}$  is the  $\text{pK}_a$  of the carbonate ion obtained from a direct reading in a  $\text{D}_2\text{O}$  solution by a  $\text{H}_2\text{O}$ -calibrated pH-meter. Knowledge of the pKa in dependence of the  $\text{D}_2\text{O}/\text{H}_2\text{O}$  mixture ratio allows calculating carbonate concentration in various  $\text{D}_2\text{O}/\text{H}_2\text{O}$  mixtures, matching the carbonate concentration at 25°C and pH 9.00 in pure  $\text{H}_2\text{O}$ . As Table S3 reveals, the results from both above-described procedures are in excellent agreement.

### ***Fourier-Transform Infrared Spectroscopy (FTIR)***

Attenuated total reflection (ATR)-FTIR spectra of the precipitated particles were recorded on a Perkin Elmer spectrometer 100 equipped with a diamond ATR crystal from 760 to 4000  $\text{cm}^{-1}$  with a resolution of 1  $\text{cm}^{-1}$ , allowing the detection of the carbonate vibrational bands denoted as  $\nu_1$ ,  $\nu_2$ ,  $\nu_3$  and  $\nu_4$ , according to the symmetric stretch, out-of-plane bending, asymmetric stretch and in-plane bending vibrational modes, respectively.

### **Rapid Scan Measurements**

Liquid state ATR-FTIR measurements were conducted utilizing a Bruker 80V spectrometer equipped with a DET ASM V27 MCT-MB600 FTIR detector and with a heated Golden Gate ATR diamond single reflection unit (Specac GS10540) equipped with ZnSe lenses. The temperature was kept constant at 25°C utilizing a build-in temperature controller and Lauda thermostat (Ecoline E300), pre-adjusting the temperature of reactants within the umbilical tubes linking a syringe pump to the ATR-FTIR stopped flow mixing cell (TgK Scientific SF-61/FT-IR) installed on top of the ATR-FTIR unit. Calcium chloride,  $\text{CaCl}_2$ , and sodium carbonate ( $\text{Na}_2\text{CO}_3$ ) (both 0.2M) were prepared in various  $\text{D}_2\text{O}/\text{H}_2\text{O}$  mixtures (12.5%, 25%, 50%, 75% and 100%  $\text{D}_2\text{O}$ ). In all experiments  $\text{D}_2\text{O}$  (99.9%) from Eurisotop was used. The calcium carbonate precursor solutions were mixed in a 1:1 volume ratio employing a custom-made ATR-FTIR stopped-flow mixing cell and 7000 scans were recorded between 650 and 1900  $\text{cm}^{-1}$  and with a spectral resolution of 4  $\text{cm}^{-1}$ .

For spectral background correction, a calcium chloride solution with the specific  $\text{D}_2\text{O}/\text{H}_2\text{O}$  ratio used in the actual precipitation experiments was recorded. Due to the width of the carbonate bands, all scans were off-set corrected between 889 and 891 wavenumbers. The time transients were extracted at 869  $\text{cm}^{-1}$  corresponding to the second derivative minimum of the  $\nu_2$  carbonate vibrational band. To facilitate direct comparison of the kinetics for each solvent isotopic composition, the maximum intensity of the  $\nu_2$  carbonate time transients was normalised to 1.

## Supplementary Tables

**Table S1.** Force field parameters of the different water models.

model	q(O)	q(H)	$\epsilon_{O-O}$	$\sigma_{O-O}$	$K_{bond}$	$b_0$	$K_{angle}$	$\theta_0$
SPC <sup>13</sup>	-0.82	0.41	0.15535	3.166	1000 <sup>b</sup>	1.0	1000 <sup>b</sup>	109.47
SPC/E <sup>8</sup>	-0.8476	0.4238	0.15535	3.166	1000 <sup>b</sup>	1.0	1000 <sup>b</sup>	109.47
SPC/HW <sup>7</sup>	-0.87	0.435	0.15539	3.16555	1649.1 <sup>b</sup>	1.0	183.07 <sup>b</sup>	109.47
SPC/fw <sup>9</sup>	-0.82	0.41	0.15542	3.16549	529.585	1.012	37.95	113.24
<b>SPC/HW/fw</b>	<b>-0.84167</b>	<b>0.420835</b>	<b>0.15542</b>	<b>3.16549</b>	<b>529.585</b>	<b>1.012</b>	<b>37.95</b>	<b>113.24</b>
SPC/fw/SM <sup>a</sup>	-0.82	0.41	0.15542	3.16549	529.585	1.012	37.95	113.24

<sup>a</sup>: scaled masses of H to D;

<sup>b</sup>: rigid model

**Table S2.**  $D_2O$  properties

	SPC/HW	SPC/HW/fw	experimental
density [ $gcm^{-3}$ ]	1.1252	1.1392	1.1044 <sup>14</sup>
$\langle \theta_{HOH} \rangle$ [ $^\circ$ ]	109.47	107.22	106 <sup>a,15</sup>
$\mu_{D_2O}/\mu_{H_2O}$	1.026	1.034	1.055 <sup>b</sup>
$\Delta_{w \rightarrow d} \langle q \rangle$ <sup>c</sup>	0.009	0.014	

<sup>a</sup>: derived from ref.<sup>15</sup> by Wu et al.<sup>9</sup>;

<sup>b</sup>: Ratio of polarizability as used by Grigera<sup>7</sup>;

<sup>c</sup>: tetrahedrality difference  $H_2O$  to  $D_2O$ .

**Table S3.** pKa values and pL values (the generalized equivalent of pH in the mixture, that is, including all the isotopically different hydrogens)<sup>11</sup> of solutions that have the same carbonate concentration as a pure 10 mM H<sub>2</sub>O solution of pH 9.00 at 25 °C.

Fraction D <sub>2</sub> O (%)	Calculated pKa according to Krężel and Bal <sup>12</sup>	pL according to Salomaa et al. <sup>11</sup>	Measured pKa (this work)	Measured pL (this work)
0	10.33	9.00	10.33	9.00
12.5	10.37	9.04	10.39	9.04
25	10.42	9.09	10.41	9.09
37.5	10.47	9.14	10.46	9.14
50	10.51	9.19	10.5	9.18
75	10.61	9.29	10.61	9.29
99	10.74	9.41	10.72	9.41

**Table S4.** Residence time of water around ions

	$t_{av}$ [ps]	$\tau_{Impey}$ [ps]	exp [ps]	other simulations
<i>Ca</i> <sup>2+</sup>				
<i>H</i> <sub>2</sub> <i>O</i>	183 ± 205	227 ± 81	<100 <sup>16,17</sup>	177-753 <sup>a,18</sup> 120.8 & 169.7 <sup>b,19</sup> ; 187.3 <sup>20</sup> ; 700 <sup>6</sup>
<i>D</i> <sub>2</sub> <i>O</i>	410 ± 518	579 ± 174		
<i>CO</i> <sub>3</sub> <sup>2-</sup>				
<i>H</i> <sub>2</sub> <i>O</i>	31 ± 32	33 ± 10		
<i>D</i> <sub>2</sub> <i>O</i>	48 ± 53	57 ± 20		

$t_{av}$  : Average residence time ± standard deviation calculated via bookkeeping

$\tau_{Impey}$  : Residence time calculated like ref.<sup>5</sup> with  $\tau^* = 2$  ps.

<sup>a</sup>: dependent on the force field & water model (in ascending order: CHARMM27, AMBER03, GROMOS87, GROMOS96);

<sup>b</sup>: dependent on the box size (CHARMM22)

## Supplementary Figures

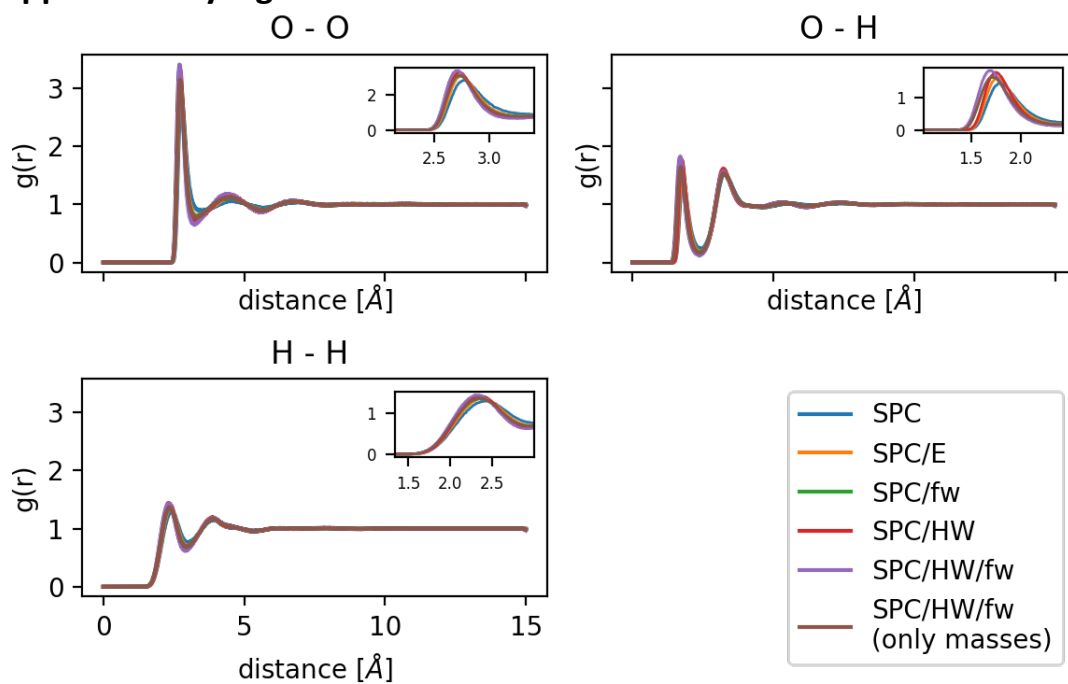


**Figure S1.** Radial distribution function of the different water models.

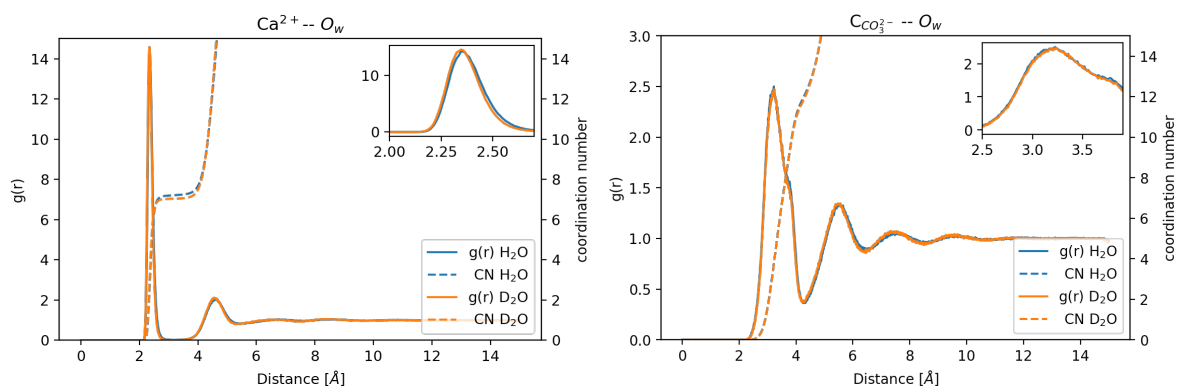


**Figure S2.** Radial distribution functions and coordination number of the ions in  $\text{H}_2\text{O}$  and  $\text{D}_2\text{O}$  as indicated.

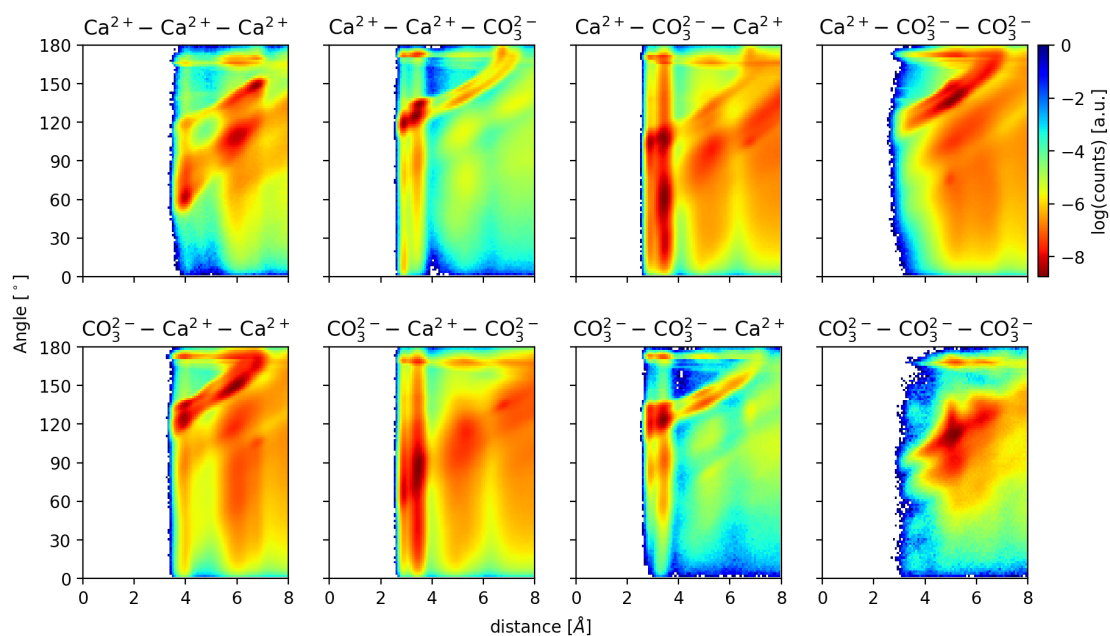


**Figure S3.** 2D histograms of angle-distance combinations for the different ion combinations within clusters in H<sub>2</sub>O.

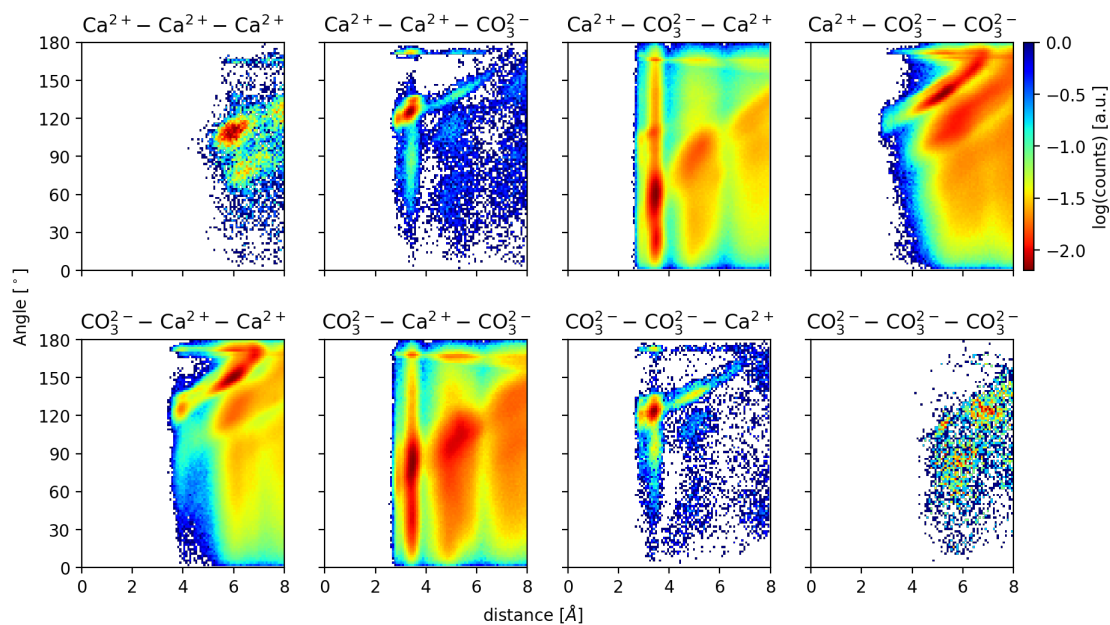


**Figure S4.** 2D histograms of angle-distance combinations for the different ion combinations within clusters in D<sub>2</sub>O.

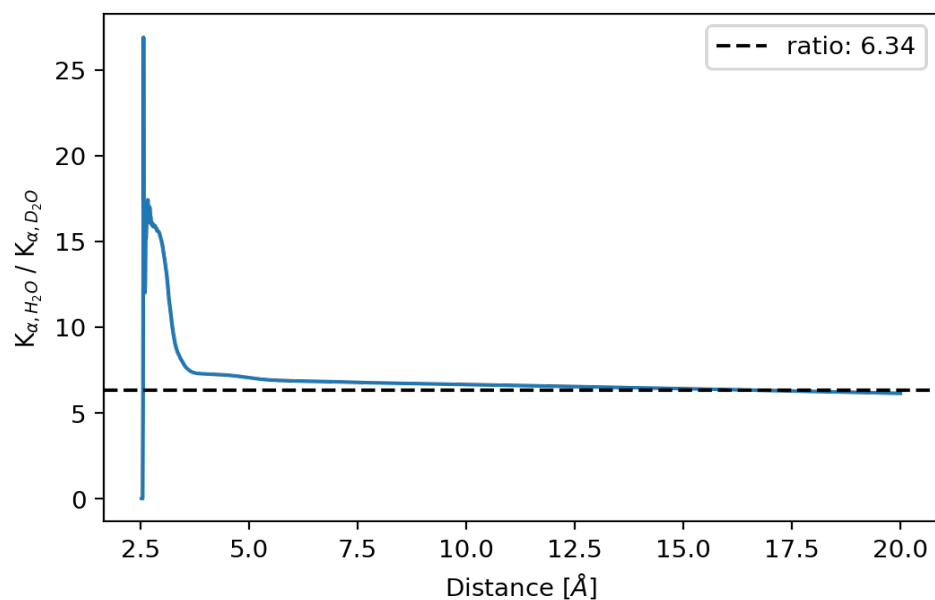


**Figure S5.** Ratio between the association constants for  $Ca^{2+}-CO_3^{2-}$  association in  $H_2O$  and  $D_2O$  as function of cut-off distance.

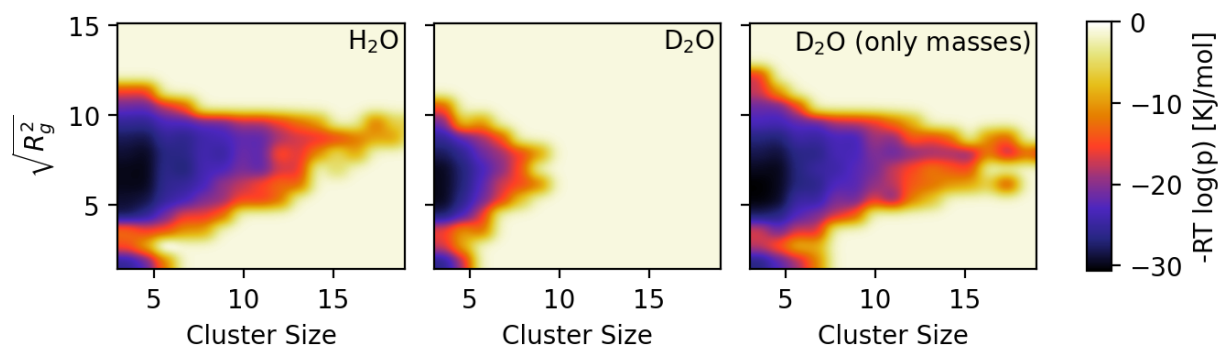


**Figure S6.** 2D histogram of the cluster size (number of ions) vs radius of gyration. From left to right:  $H_2O$ ,  $D_2O$ ,  $H_2O$  with masses scaled to  $D_2O$ .

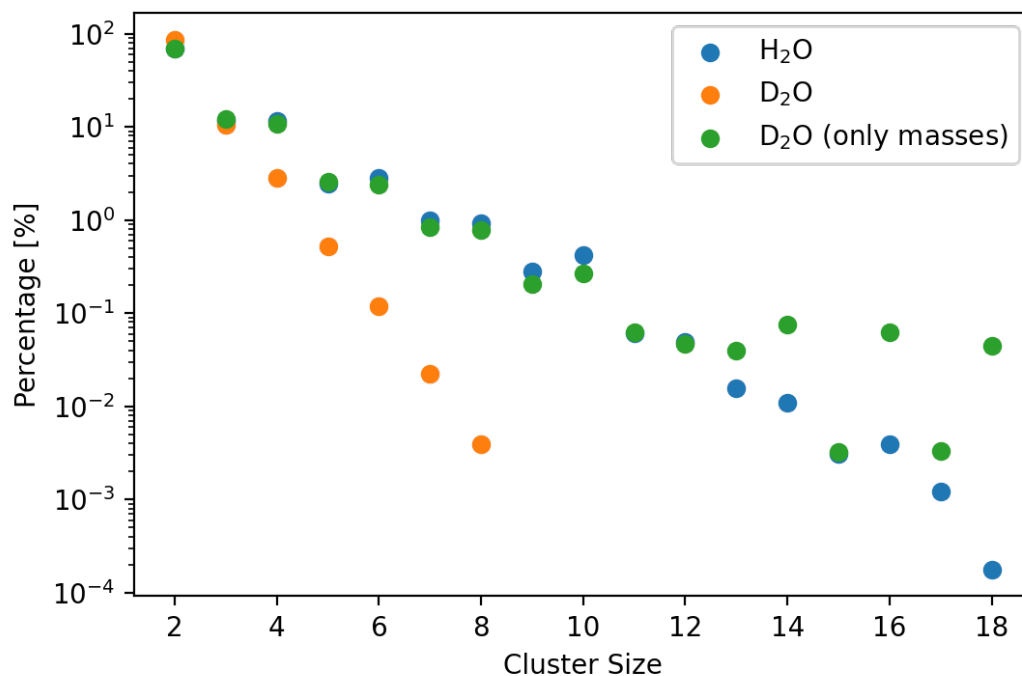


**Figure S7.** Histogram of the cluster size for simulations in  $H_2O$ ,  $D_2O$ ,  $H_2O$  with masses scaled to  $D_2O$  (“pseudo- $D_2O$ ”).

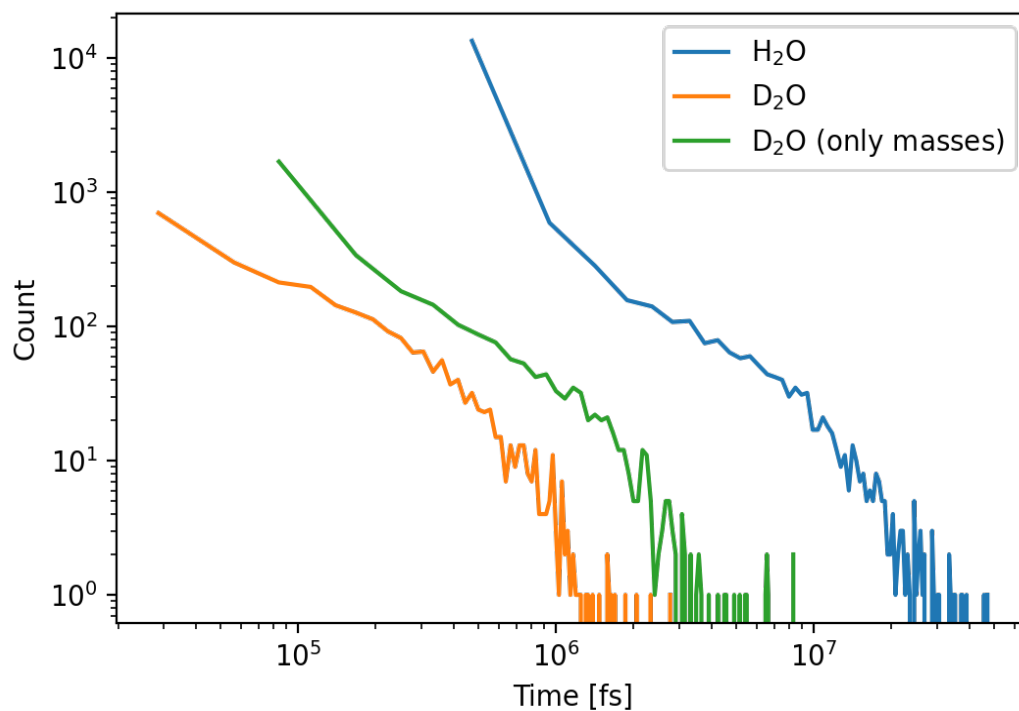


**Figure S8.** Histogram of the cluster lifetimes for simulations in  $H_2O$ ,  $D_2O$ ,  $H_2O$  with masses scaled to  $D_2O$  (“pseudo- $D_2O$ ”).

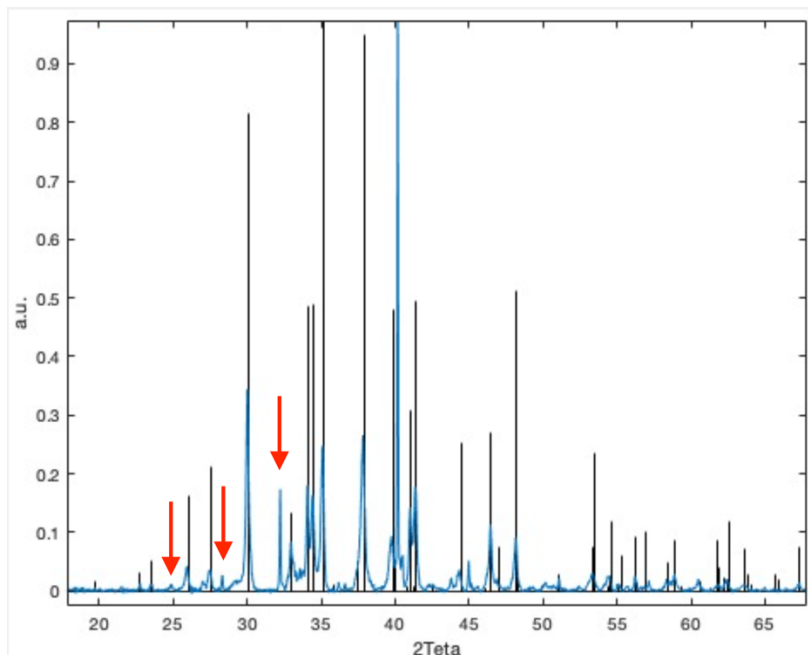


**Figure S9.** XRD analysis of a sample quenched from a titration performed in 75% D<sub>2</sub>O in light water. Once the post-nucleation plateau was reached, samples were quenched in absolute ethanol, stirred for 30min, let to decant for 30min and dried in a vacuum oven for 2h. The experimental data is the blue line, black vertical lines represent the literature reflexes for sodium carbonate. Red arrows indicate reflexes that we could not assign to any crystalline form that can form in this system.

## References

- 1 P. Raiteri, R. Demichelis and J. D. Gale, *The Journal of Physical Chemistry C*, 2015, **119**, 24447–24458.
- 2 W. Shinoda, M. Shiga and M. Mikami, *Phys. Rev. B*, 2004, **69**, 134103.
- 3 M. E. Tuckerman, J. Alejandre, R. López-Rendón, A. L. Jochim and G. J. Martyna, *Journal of Physics A: Mathematical and General*, 2006, **39**, 5629–5651.
- 4 R. W. Hockney and J. W. Eastwood, *Computer simulation using particles*, A. Hilger, Bristol [England] ; Philadelphia, Special student ed., 1988.
- 5 R. W. Impey, P. A. Madden and I. R. McDonald, *J. Phys. Chem.*, 1983, **87**, 5071–5083.
- 6 S. Koneshan, J. C. Rasaiah, R. M. Lynden-Bell and S. H. Lee, *The Journal of Physical Chemistry B*, 1998, **102**, 4193–4204.
- 7 J. R. Grigera, *The Journal of Chemical Physics*, 2001, **114**, 8064–8067.
- 8 H. J. C. Berendsen, J. R. Grigera and T. P. Straatsma, *J. Phys. Chem.*, 1987, **91**, 6269–6271.
- 9 Y. Wu, H. L. Tepper and G. A. Voth, *The Journal of Chemical Physics*, 2006, **124**, 024503.
- 10 A. Glättli, PhD Thesis, ETH Zurich, 2004.
- 11 Pentti. Salomaa, L. L. Schaleger and F. A. Long, *J. Am. Chem. Soc.*, 1964, **86**, 1–7.
- 12 A. Krężel and W. Bal, *Journal of Inorganic Biochemistry*, 2004, **98**, 161–166.
- 13 D. Eisenberg and W. Kauzmann, *The Structure and Properties of Water*, Oxford University Press, 2005.
- 14 D. R. Lide, Ed., *CRC Handbook of Chemistry and Physics, 89th Edition*, Taylor & Francis Ltd., 89th edn., 2019.
- 15 K. Ichikawa, Y. Kameda, T. Yamaguchi, H. Wakita and M. Misawa, *Molecular Physics*, 1991, **73**, 79–86.
- 16 P. S. Salmon, W. S. Howells and R. Mills, *Journal of Physics C: Solid State Physics*, 1987, **20**, 5727–5747.
- 17 H. Ohtaki and T. Radnai, *Chemical Reviews*, 1993, **93**, 1157–1204.
- 18 Y. Lee, D. Thirumalai and C. Hyeon, *J. Am. Chem. Soc.*, 2017, **139**, 12334–12337.
- 19 S. Obst and H. Bradaczek, *J. Phys. Chem.*, 1996, **100**, 15677–15687.
- 20 S. Mamatkulov and N. Schwierz, *The Journal of Chemical Physics*, 2018, **148**, 074504.